IJST, Transactions of Mechanical Engineering, Vol. 38, No. M1+, pp 207-215
Printed in The Islamic Republic of Iran, 2014

EVALUATION OF SENSITIZATION IN GAS TUNGSTEN ARC WELDED AISI 304 STAINLESS STEEL*

M. ROSHANI[1], M. REIHANIAN[2], KH. GHEISARI[3**], AND M.R. SAFFARIAN[4]

[1, 2,3]Dept. of Materials Science and Eng., Faculty of Eng., Shahid Chamran University of Ahvaz, I. R. of Iran
Email: khgheisari@scu.ac.ir
[4]Dept. of Mechanical Eng., Faculty of Eng., Shahid Chamran University of Ahvaz, I. R. of Iran

Abstract– In this study, the temperature distribution of an AISI 304 stainless steel during gas tungsten arc welding is modeled by using the Goldak's three-dimensional moving heat source. A C++ program is developed in order to employ the heat inputs into finite difference thermal simulation of the welded plate. By simulating the temperature distribution and shape of the weld pool, effect of welding parameters such as current and welding speed on the sensitization, weld width and weld depth are evaluated. Results show that the width and depth of weld and sensitized zone increase with raising the current while the sensitization location decreases. The effect of welding speed is vice versa. To verify the simulated results, currents of 160, 200 and 240 A and welding velocity of 2 mm/s are selected for experiments. Good agreement is obtained between the simulated and experimental results.

Keywords– Stainless steel, welding, sensitization, modeling

1. INTRODUCTION

Austenitic stainless steels are categorized as the largest group of stainless steels and widely used in various industries because of their excellent corrosion resistance [1]. One problem that arises during welding of austenitic stainless steels is sensitization in heat-affected zone that leads to intergranular corrosion [2]. Sensitization takes place in the area that experiences peak temperatures of 650 ◦C to 900 ◦C for a number of seconds during the welding [3]. It occurs because chromium rich carbides and intermetallic phases precipitate along grain boundaries. Adjacent to the carbides, a chromium-depleted zone is formed that can be preferentially attacked in corrosive environment.

Sensitization has been investigated experimentally by numerous researchers [2], only a few of them are referred in Refs. [4-6] as examples. There have also been some efforts to model the sensitization in stainless steels [7-12]. Mozhi et al. [7-8] used a thermodynamic model to investigate the sensitization in stainless steels. Yu and Chen [9] developed a cellular automaton model to investigate the kinetics of carbides precipitation and the three dimensional distribution of Cr concentration. Yu et al. [10] also adopted a cellular automaton modeling to simulate the recrystallization under different deformations. Sahlaoui et al. [11] developed an analytical model to predict the profiles of chromium depleted zones and found a good agreement with experimental results. Jain et al [12] investigated the spread of intergranular corrosion using micrometer scale simulations and experimental verifications on sensitized stainless steel. These models consider the sensitization in a process other than welding while the sensitization of austenitic stainless steel during welding has not been modeled or simulated yet.

*Received by the editors January 9, 2013; Accepted January 20, 2014.
**Corresponding author

There are a number of tools to model the welding process [13-15]. Development of model tools is based on the analysis of thermal history during welding and considering the effect of processing parameters on temperature distributions. The basic theory of heat flow has been applied by Rosenthal [16] to moving heat sources. It is an analytical way for calculating the thermal history of the welds. Rosenthal's analysis supposes a point, line, or plane source. It assumes the infinite temperature at the heat source and ignores the temperature dependence of the thermal properties. Pavelec et al. [17] proposed a distributed heat source with Gaussian distribution of heat flux on the surface of the plate. Goldak and his coworkers [18] developed a non-axisymmetric three-dimensional heat source model. This model is more realistic and flexible than any other model so far proposed for weld heat sources. It utilized the finite element modeling to calculate the temperature field and showed that the three-dimensional heat source could overcome the shortcomings of the previous two-dimensional Gaussian model to predict the temperature of the welded joints with much deeper penetration.

The present paper is an attempt to model the sensitization in gas tungsten arc welded AISI 304 stainless steel. Goldak's three-dimensional moving heat source model [18] is considered by using the finite difference method. The welding parameters affecting the heat distribution in gas tungsten arc welding are evaluated by simulation. The size and location of the sensitization zone are predicted. The width and depth of the weld is also envisaged. The validity of the model is checked by experiments by means of some typical welding parameters.

2. MATERIAL AND METHODS

A commercial 304 type austenitic stainless steel was used throughout this study. Table 1 shows the chemical composition analysis of the material used. Although a variety of welding techniques with different parameters and heat inputs are practically applied to austenitic stainless steels, one-pass gas tungsten arc welding without filler materials was adopted for simplicity in the present study. The base material with dimensions of 100×100×10 mm^3 was welded by bead-on-plate gas tungsten arc welding at a welding current of 160A to 240A in direct current electrode negative (DCEN), a travel speed of 2-4 mm/s and the arc length of 2 mm without filler materials with argon gas for shielding. The ambient temperature was 17°C. The welding parameters are listed in Table 2. For experiments, the welding conditions of sample 2 are selected and regarded as the reference sample. To verify the size and the location of the sensitization zone, the weld cross section was etched in 10% oxalic acid. Measurements were conducted under an optical microscope at 200-times magnification. The sensitization zone was defined as the region in which more than 30% of the grain boundaries were attacked [2].

Table 1. Chemical Composition of the material used for this study

Element	Fe	C	Cr	Mo	Ni	Mn	Si	Cu	P	S
Wt.%	Balanced	0.055	18.5	0.21	9.35	0.99	0.43	0.78	0.045	0.015

Table 2. Experimental welding parameters chosen for this study

Sample	Current (A)	Velocity (mm s^{-1})	Voltage (V)	Polarity	Ambient Temperature (^oC)
1	160	2	15	DCEN	17
2	200	2	15	DCEN	17
3	240	2	15	DCEN	17
4	200	4	15	DCEN	17

3. GOLDAK'S DOUBLE-ELLIPSOID MODEL

For the thermal analysis of a weld, the magnitude and distribution of the heat input from the welding arc are required. The temperature distributions and variations during gas tungsten arc welding are predicted by the finite difference method. According to the Goldak's model [18], two ellipsoidal sources (one in the front quadrant of the heat source and the other in the rear quadrant) are combined as shown in Fig. 1. The power density inside the front quadrant of the double ellipsoid heat source, *qf(x, y, z)*, is:

$$q_f(x,y,z) = f_f \frac{6\sqrt{3}}{abc_f}\frac{Q_s}{\pi\sqrt{\pi}}\exp(-3(\frac{x}{a})^2)\exp(-3(\frac{y}{b})^2)\exp(-3(\frac{z}{c_f})^2) \quad (1a)$$

and for the rear quadrant, *qr(x, y, z)*, is

$$q_r(x,y,z) = f_r \frac{6\sqrt{3}}{abc_r}\frac{Q_s}{\pi\sqrt{\pi}}\exp(-3(\frac{x}{a})^2)\exp(-3(\frac{y}{b})^2)\exp(-3(\frac{z}{c_r})^2) \quad (1b)$$

where $Q_S = I.U.\eta$ is the energy input rate determined by the product of welding current I, voltage U and efficiency η. f_f and f_r are the fractions of the heat deposited in the front and rear quadrants and are established by $f_f + f_r = 2$ [18]. The constants, a, b, c_f and c_r are heat source parameters. x, y, z are distances from heat source center and depend on the location of the electrode. Equations (1a) and (1b) indicate that Goldak's heat source model is defined as a function of position, time and a number of parameters that affect the heat flux amount and distribution.

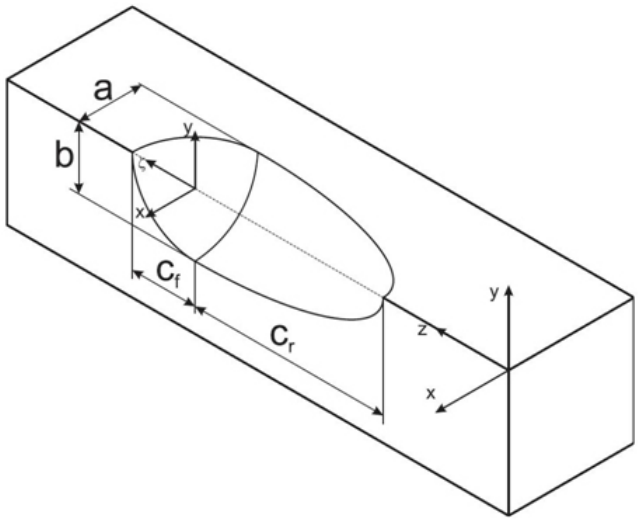

Fig. 1. Schematic model of the Goldak's double-ellipsoid heat source. Two ellipsoidal sources (one in the front quadrant of the heat source and the other in the rear quadrant) are combined

4. RESULTS AND DISCUSSION

a) Simulation

The variables determining the location and width of the sensitization zone are peak temperature distribution and the time spent between these temperatures. Figure 2 shows the temperature distribution at current of 200A during welding in the Y-Z cross section. Welding is done at the middle of plate and in the positive Z-axis direction. It is observed that the temperature in the region of the torch reaches to more than 2000 K, indicating that the material in the fusion zone is melted. In the vicinity of the fusion zone, high temperatures are present defining the heat affected zone. A small area in front of the torch where the heat

source is going to pass, is warmed by the torch. The heat inputs are slowly transferred by three modes: conduction, convection and radiation. The temperature around the edge where the welding is initiated is reduced notably to the range of 600–800 K.

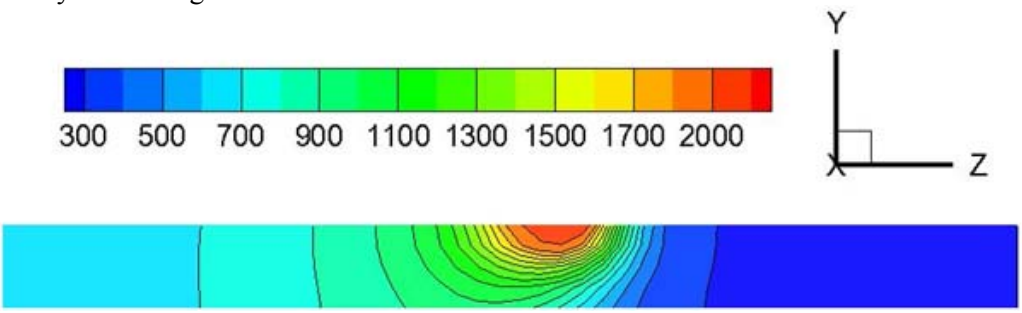

Fig. 2. Temperature distribution at current of 200A during welding in the Y-Z cross section of the welded plate. All temperatures are in Kelvin (K)

Figure 3 shows the temperature distribution as a function of time for welding current of 200A and different distances from the weld pool. The filled area indicates the temperature range of sensitization that is about 900 to 1150 K. For distances very close to the weld line, the temperature gradient is sharp during warming and cooling. Therefore, there is not enough time to form any precipitation. On the other hand, for distances far away from the weld line (7 mm from weld line and more) the increase in temperature is not enough for precipitation to occur. Nevertheless, at intermediate distances (around 5 mm from the weld string) the temperature rise and time are sufficient for precipitation of the carbides. These areas are prone to sensitization.

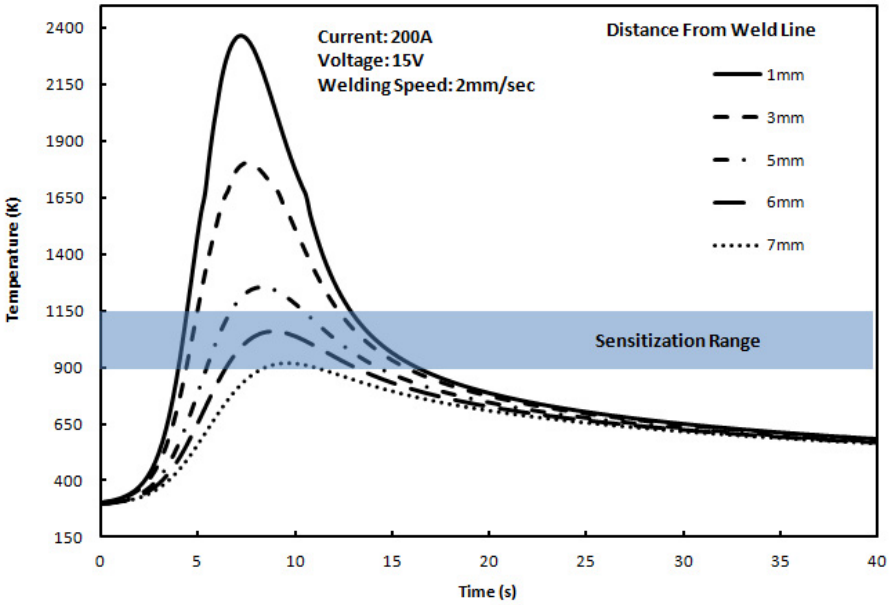

Fig. 3. Temperature variations at different locations from the weld line. The filled area shows the temperature range of sensitization (900 to 1150 K)

The exposure time to the temperature range of sensitization can be determined by Fig. 3. These periods are shown in Fig. 4 for current of 200 A, voltage of 15 V and welding speed of 2 mm/s. These diagrams can be drawn for different welding parameters. For an AISI 304, sensitization occurs in the region that experiences this range of temperature for about 7 seconds [19]. Using this criterion and employing Fig. 4, the size and location of the sensitization can be determined. For the present conditions, a 0.43 mm wide sensitization zone occurs at the distance of 5.39 mm away from the weld line.

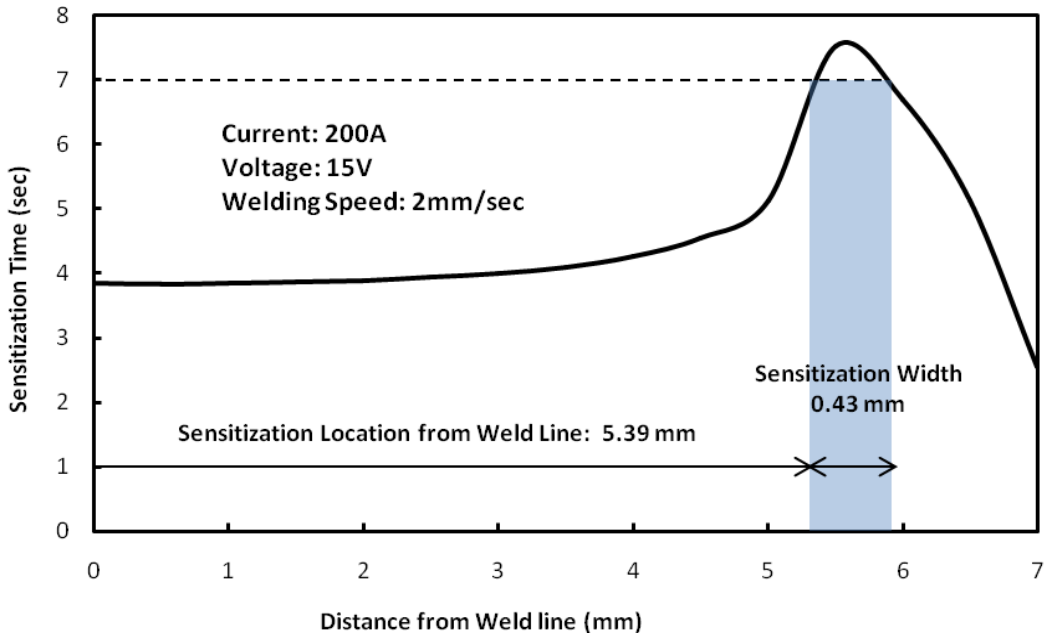

Fig. 4. The exposure time to the temperature range of sensitization as a function of the distance from weld line. For the present conditions, a 0.43 mm wide sensitization zone occurs at the distance of 5.39 mm away from the weld line

Figure 5 shows the effect of welding current on the size and location of the sensitization zone as well as the weld depth and width. It is seen that the depth and width of the weld increases as the current is raised. The sensitization size increases as well. However, sensitization becomes closer to the weld line with increasing the welding current. According to Fig. 5, to reduce the size of sensitization, the current should be low as possible. However, as the results indicate, the weld depth is reduced by choosing low values of the current. Considering that the plate thickness is 10 mm, the weld depth must be at least 3 mm (indicated by the dashed line). Therefore, the lowest value of the current that can satisfy this condition is 195 A.

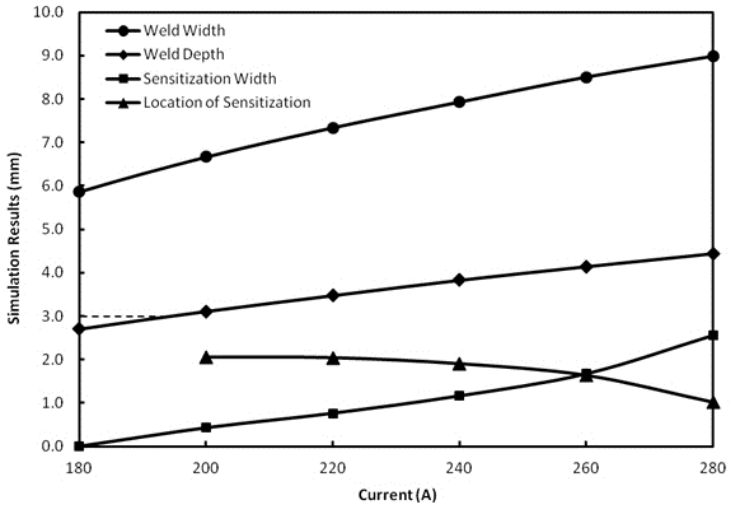

Fig. 5. Weld depth, weld width, sensitized size and its location from weld line as a function of welding current. The size of sensitization increases and the sensitization comes closer to the weld line with the increase in the depth and width of the weld

The effect of the welding speed on the weld depth, weld width, sensitization location and its size is illustrated in Fig. 6. It is observed that the welding speed has an inverse effect compared to the welding

current. That is, weld depth, weld width and sensitized region shrink while the sensitized location becomes farther from the weld line as the welding speed is increased. Enhancing the welding speed means that the heat source is applied for a shorter period. Consequently, the temperature of the whole plate becomes lower, resulting in a thinner weld depth and width. The sensitization location is also increased. On the other hand, the carbides have lower times to precipitate on grain boundaries that lead to forming a narrower sensitized region. According to Fig. 6, the sensitized zone is approximately eliminated for welding speeds greater than 2 mm/s. However, the welding speed should be high enough to have a suitable weld depth (3 mm for the thickness of 10 mm).

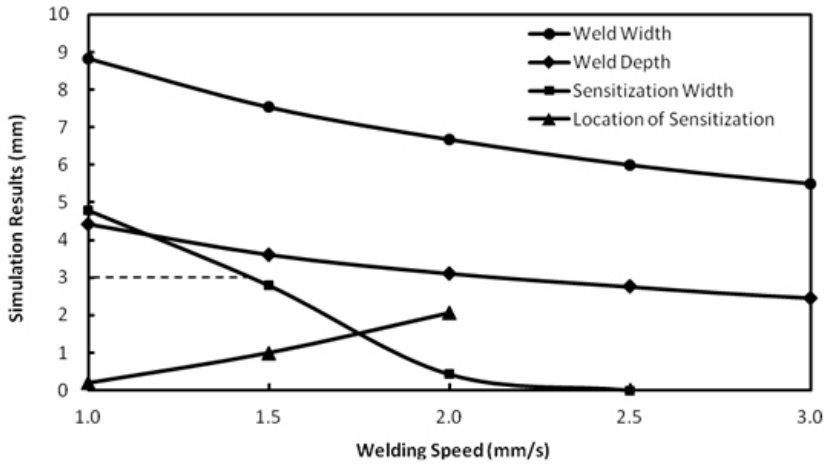

Fig. 6. Weld depth, weld width, sensitized size and its location from weld line as a function of welding speed. The sensitization size decreases and the sensitized location becomes farther from the weld line as the welding speed is increased

In summary, to eliminate the sensitized region, high-speed and low-current welding is required. It is consistent with the experimental work of Tsai and Eagar [3]. However, to have a reasonable weld depth, the highest welding speed and the lowest welding current must be 2 mm/s and 195 A, respectively.

b) Experimental

As mentioned in section 3, the welding parameters of sample 2 are considered for experiments. The experimentally obtained weld pool shape for sample 2 is shown in the right part of Fig. 7. For comparison, the simulated results are also included on the left. Good agreement is observed for the weld pool and fusion line. Moreover, the weld depth and weld width are measured experimentally for the conditions summarized in Table 3. The corresponding, simulated results are also included. The welding velocity for sample 4 is 4 mm/s, which is beyond the critical. Therefore, the weld depth and weld width of the sample 4 are not pointed out in the Table. The results of Table 3 indicated that the experimental results confirm the numerical calculations with only a few errors.

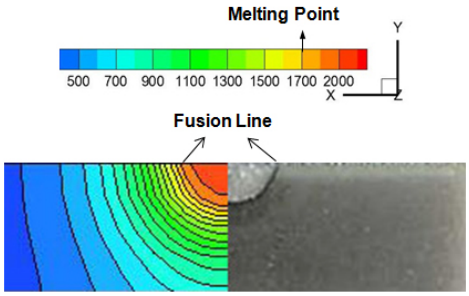

Fig. 7. Simulated and experimental weld pool obtained for sample 2, indicating a good agreement between the experimental and simulated data

Table 3. Simulation and experimental values of the weld width and weld depth

Sample	Current (A)	Velocity (mm s^{-1})	Simulation		Experimental	
			Weld Width (mm)	Weld Depth (mm)	Weld Width (mm)	Weld Depth (mm)
1	160	2	4.94	2.23	4.5	2.6
2	200	2	6.67	3.11	6.7	3
3	240	2	7.93	3.83	8.3	4.1
4	200	4	---	---	---	---

Table 4. Simulation and experimental values of the sensitized size and its location from weld line

Sample	Current (A)	Velocity (mm s^{-1})	Simulation		Experimental	
			Sensitized Size (mm)	Sensitized distance (mm)	Sensitized Size (mm)	Sensitized distance (mm)
1	160	2	---	---	---	---
2	200	2	0.43	2.01	0.5	2.1
3	240	2	1.16	1.90	1	2
4	200	4	---	---	---	---

The metallographic images obtained from the sensitized zone of sample 2 are presented in Fig. 8 for two magnifications. Thick grain boundaries indicate the precipitation of carbides in the sensitized region. Fig. 9 shows the metallographic images of sample 1, 2 and 3 at different welding conditions (see Table 2). Each figure consists of four images taken from particular locations away from the weld line. No sensitized region is observed in sample 1, which is consistent with the simulated results. However, in sample 2 and 3 thick grain boundaries indicating the sensitized zone are seen. These zones are located a short distance from the weld line. Table 4 summarized the simulated and experimentally measured values of the sensitized width and its location from the weld line for different welding conditions. For sample 1 and 4, sensitization does not appear. Thus, its size and location is not mentioned in the Table. In spite of only a few errors, experimental results confirm the simulation.

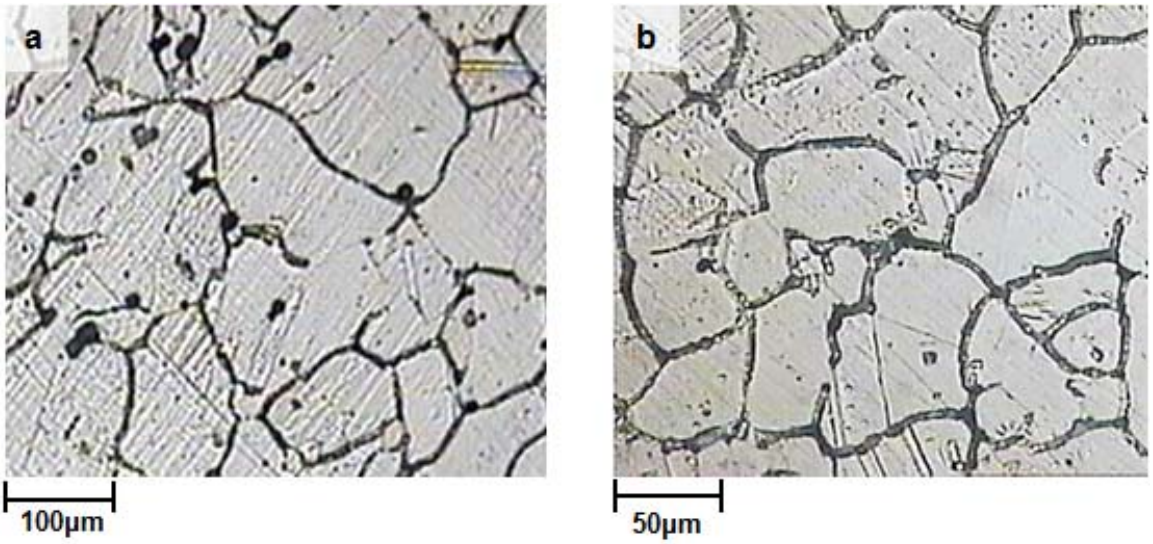

Fig. 8. Microscopic images taken from the sensitized zone in sample 2 at low (a) and high (b) magnifications. Formation of the chromium carbide along the austenite grain boundaries leads a chromium-depleted zone adjacent to the austenite grain boundary

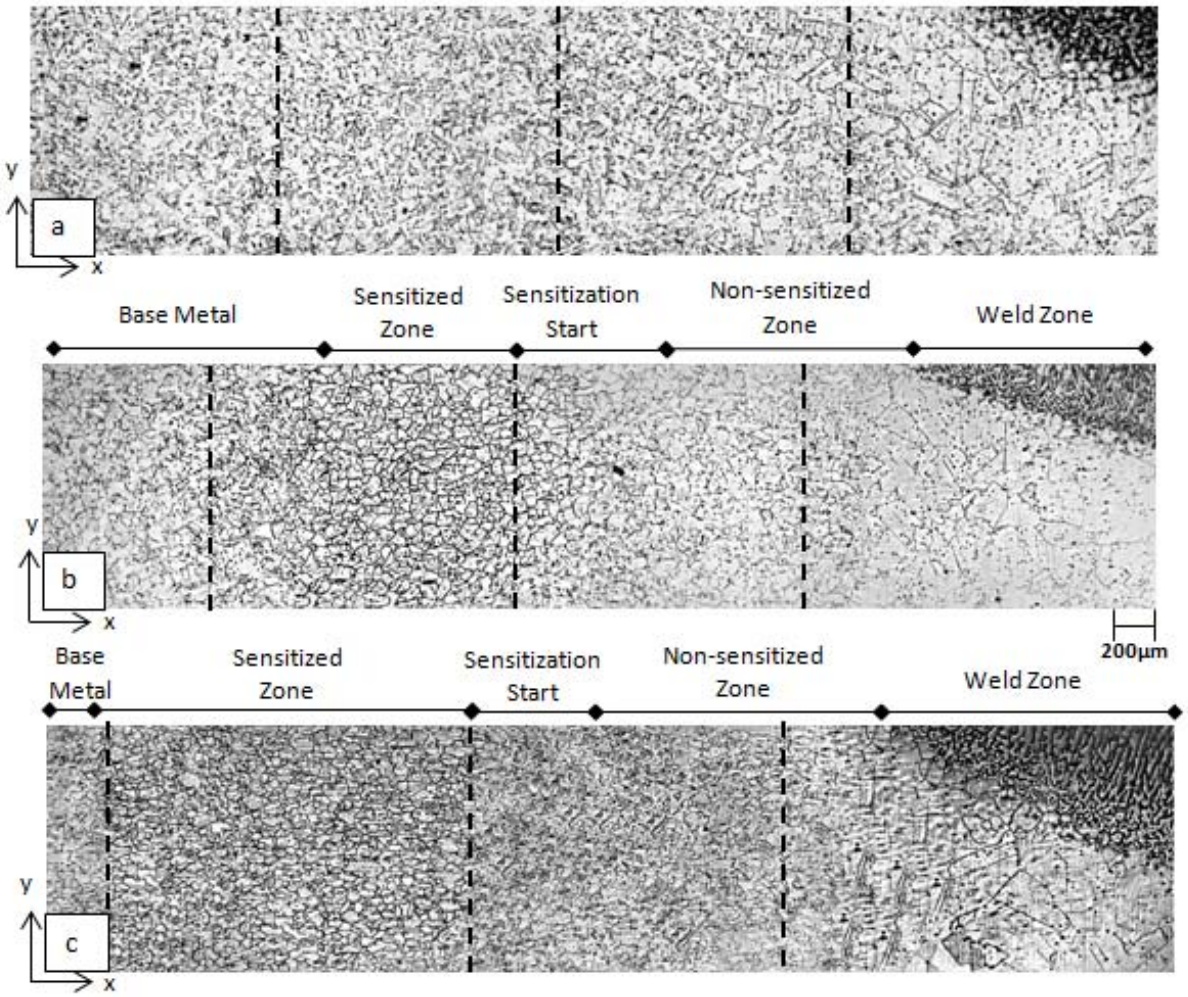

Fig. 9. Microscopic images at different locations from weld line a) sample 1, b) sample 2 and c) sample 3. Each figure consists of four images taken from particular locations away from the weld line. Thick austenite grain boundaries in sample 2 and 3 indicate the precipitation of Cr carbide at the grain boundaries, which is called sensitization

5. CONCLUSION

1- Weld depth, weld width and sensitized area increase with increasing the welding current. The effect of welding speed is reversed.

2- To eliminate the sensitized region, high-speed and low-current welding is required.

2- To have a reasonable weld depth, the highest welding speed and the lowest welding current must be 2 mm s^{-1} and 195 A, respectively.

3- Metallographic images reveal the sensitization in the welds with the current of 200 A and 240 A, voltage of 15 V and the speed of 2 mm/s.

4- Good conformity is observed between the experimental and simulated results of weld depth and width and sensitized size and location.

Acknowledgments: The authors would like to thank Shahid Chamran University for their financial support through the Grant Number 89-3-02-44305. M. Roshani also appreciates Mr. Ostovar and Mrs. Babadi, for their support and useful discussions.

REFERENCES

1. Lippold, J. C. & Kotecki, D. J. (2003). *Welding metallurgy and weldability of stainless steels*. 1st edn, John Wiley & Sons Inc., New Jersey.
2. Dayal, R. K., Parvathavarthini, N. & Raj, B. (2005). Influence of metallurgical variables on sensitisation kinetics in austenitic stainless steels. *Int. Mater. Rev*., Vol. 50, pp. 129-155.
3. Tsai, N. S. & Eagar, T. W. (1984). The Size of the sensitization zone in 304 stainless steel welds. *J. Mater. Energy Syst*., Vol. 6, pp. 33-37.
4. Singh, R., Das, G., Singh, P. K. & Chattoraj, I. (2009). Low temperature sensitization behavior of base, heat-affected zone and weld pool in ASIS 304 L. *Metall. Trans*., Vol. 40A, pp. 1219-1234.
5. Hamada I. & Yamauchi, K. (2002). Intergranular stress corrosion cracking behavior of types 308 and 316 stainless steel weld metals in simulated boiling water environment. *Metall. Trans*., Vol. 33A, pp. 2907-2919.
6. Moura, V., Kina, Y. A., Tavares, M. M. S., de Faria, G. & Mainier, F. B. (2009). Investigation of cracks and sensitization in an AISI 304L stainless steel exposed to 500–600º C. (2009). Eng. Fail. Anal., Vol. 16, pp. 545–551.
7. Mozhi, T. A., Betrabet, H. S., Jagannathan, V., Wilde, B. E. & Clark, W. A. T. (1968). Thermodynamic modeling of sensitization of AISI 304 stainless steels containing nitrogen. *Scripta Metall*., Vol. 20, pp. 723-728.
8. Mozhi, T. A., Juhas, M. C. & Wilde, B. E. (1987). Modeling low temperature sensitization of austenitic stainless steels. *Scripta Metall*., Vol. 21, pp. 1547-1552.
9. Yu, X. & Chen, S. (2009). A simulation of Cr depletion in austenitic stainless steel with cellular automaton. *Comput. Mater. Sci*., Vol. 45, pp. 899–904.
10. Yu, X., Chen, S. & Wang, L. (2009). Simulation of recrystallization in cold worked stainless steel and its effect on chromium depletion by cellular automaton. *Comput. Mater. Sci*., Vol. 46, pp. 66-72.
11. Sahlaoui, H., Makhlouf, H., Sidhom, H. & Philibert, J. (2004). Effects of aging conditions on the precipitates evolution, chromium depletion and intergranular corrosion susceptibility of AISI 316L: experimental and modeling results. *Mater. Sci. Eng*., Vol. 372A, pp. 98-108.
12. Jain, S., Budiansky, N. D., Hudson, J. L. & Scully, J. R. (2010). Surface spreading of intergranular corrosion on stainless steels. *Corr. Sci*., Vol. 52, pp. 873-885.
13. Satheshi, M. & Edvin Raja Dhas, J. (2013). Multi objective optimization of flux cored arc weld parameters using fuzzy based desirability function. *Iranian Journal of Science & Technology, Transactions of Mechanical Engineering*, Vol. 37, No. M2, pp. 175-187.
14. Nami, M. R., Kadivar, M. H. & Jafarpur, K. (2004). Modelling and prediction of process parameters in explosive welding of plates using GMDH-type neural network and singular value decomposition. *Iranian Journal of Science & Technology, Transaction B: Engineering*, Vol. 28, pp. 467-478.
15. Nariman- zadeh, N. & Darvizeh, A. (2002). 3D thermo-viscoplastic modeling of welds: effect of piece-wise welding on thermo-mechanical response of thick plate weldments. *Iranian Journal of Science & Technology, Transaction B: Engineering*, Vol. 26, pp. 455-464.
16. Rosenthal, D. (1941). Mathematical theory of heat distribution during welding and cutting. *Welding J*., Vol. 20, pp. 220s–34s.
17. Pavelec, V., Tanbakuchi, R., Uyehara O. A. & Myers, P. S. (1969). *Experimental and computed temperature histories in gas tungsten-arc welding of thin plates*. Welding J. Res. Suppl., Vol. 48, pp. 295–305.
18. Goldak, J., Chakravarti, A. Bibby, M. (1984). A new finite element model for welding heat source. *Metall. Trans*. Vol. 15B, pp. 299–305.
19. Kou, S. (2003). *Welding metallurgy*. 2nd ed., John Wiley & Sons Inc., New Jersey.